Electronic Supplementary Material (ESI) for Materials Advances.

Supporting Information

In situ growth of SeO_x film on the surface of Ni-Fe-selenide nanosheets as highly active and stable electrocatalysts for oxygen evolution reaction

Xiaonan Shang,[a] Weiheng Chen,[b] Zhong-Jie Jiang,[c,*] Changsheng Song,[a,*] and Zhongqing Jiang [a,*]

[a] Key Laboratory of Optical Field Manipulation of Zhejiang Province, Department of Physics, Zhejiang Sci-Tech University, Hangzhou 310018, P. R. China. E-mail: zhongqingjiang@zstu.edu.cn

[b] Department of Mechanical Engineering, Ningbo University of Technology, Ningbo 315336, P. R. China.

[c] Guangdong Engineering and Technology Research Center for Surface Chemistry of Energy Materials & Guangzhou Key Laboratory for Surface Chemistry of Energy Materials, New Energy Research Institute, College of Environment and Energy, South China University of Technology, Guangzhou 510006, P. R. China. Email: eszjiang@scut.edu.cn and zhongjiejiang1978@hotmail.com

This PDF file includes:

1. Experimental section

1.1 Chemicals

Hydrochloric acid (HCl, AR, 36.0−38.0%), ethanol (C_2H_5OH, 99.7%), nickel(II) nitrate hexahydrate ($Ni(NO_3)_2·6H_2O$, 98%, Sigma-Aldrich), urea (CH_4N_2O, ≥ 99.5%, Sigma-Aldrich), selenium powder (Se, 99.9%, Sigma-Aldrich), hydrazine hydrate ($N_2H_4·H_2O$, ≥98%, Alfa Aesar), potassium hydroxide (KOH, ≥85.0%, Alfa Aesar), and NiFe foam (thickness: 1.2 mm) were used as received. Commercial platinum/carbon (Pt/C, 20 wt.% Pt loading on carbon black, Johnson Matthey). Iridium black (Ir, 99.95%) was purchased from Alfa Aesar. Deionized water through Millipore system (Milli-Q®) was used.

1.2 Electrocatalytic measurements

All electrochemical measurements were performed at room temperature in a standard three-electrode system by electrochemical workstation (CHI760E), using a Pt foil as the counter electrode, a saturated calomel electrode (SCE) as the reference electrode, and the NiFe foam supported $SeO_x/FeNi_xSe$ as the working electrode. Potentials vs. RHE are calculated using the equation: $E_{vs.RHE}=E_{vs.SCE}+1.068$ V in 1.0 M KOH. All the linear sweep voltammograms (LSV) were corrected by eliminating 95% IR compensation. All the OER tests were conducted from 0.191-0.791 V vs. SCE with a scan rate of 5 mV s^{-1}, and the HER LSV curves were tested from -0.8 to -1.668 V vs. SCE with a scan rate of 10 mV s^{-1}. And the corresponding Tafel plots were derived from LSV curves according to the Tafel simi-exponential equation: $\eta=b\times\log|j|+a$. Electrochemical impedance spectroscopy was measured in the frequency range of 10^{-2} to 10^5 Hz with an AC perturbation potential of 5 mV. The electrochemical stability of $SeO_x/FeNi_xSe$ (CMy-$FeNi_xSe$) electrode was investigated by chronopotentiometry and multi-step chronopotentiometric tests. For comparison, Ir (loaded on NiFe foam), FeNi LDH, FeNi-LDH after HER electrochemical modification (CMy-FeNi LDH), NiFe Foam and NiFe Foam after HER electrochemical modification (CMy-NiFe Foam) electrodes were also prepared for OER

measurement. The effective electrochemical active surface area (ECSA) of the materials was proportional to the geometric double layer capacitance (C_{dl}), which can be characterized by CV curves at various scan rates (10, 20, 30, 40, 50, 60, 70, 80, 90, 100 mV s^{-1} from 0.18 V to 0.28 V vs. RHE were used). The C_{dl} was estimated by plotting the current densities difference ($\Delta j = j_{anodic} - j_{cathodic}$) at the middle potential vs. scan rate. The resulting linear slope is twice that of the C_{dl}. The corresponding ECSA were calculated according to the following equation:

$$\mathrm{ECSA} = \frac{C_{dl}}{C_s}\ \mathrm{cm}^2 \quad (1)$$

Where, C_s is the specific capacitance, and 0.040 mF cm^{-2} was adopted as the C_s value as regared to previous reports.[1]

The performance of the overall water splitting was conducted by a two-electrode system, using Pt/C (loaded on NiFe Foam) as the cathode and the NiFe foam supported $SeO_x/FeNi_xSe$ as the anode.

1.3 Theoretical calculation details

Theoretical calculations have been performed within the framework of density functional theory (DFT) as implemented by the Vienna an initio Simulation Package (VASP).[2, 3] The exchange-correlation energy was treated in the generalized-gradient approximation (GGA) using Perdew-Burke-Ernzerhof (PBE) method.[4] The nano-model was constructed on the *z* direction of $Ni_{1-x}Fe_xSe$ ($Ni_{26}Fe_1Se_{27}$), $Ni_{1-x}Fe_xSe@SeO_2$ ($Ni_{26}Fe_1Se_{27}@Se_8O_{16}$) with 16 Å vacuum. The cutoff energy of plane wave was chosen at 450 eV. For the structure optimizations, 4×4×1 Monkhorst-Pack (MP) grids were used. The changes in total energies between two successive iteration steps were less than 10^{-5} eV, and all the Hellmann-Feynman force acting on each atom was lower than 0.01 eV /Å. The adsorption free energies of O, *OH and *OOH on all structures were calculated by the formula $\Delta G = \Delta E + \Delta ZPE - T\Delta S$, where ΔE, ΔZPE, ΔS are the binding energy, zero point energy change and entropy change of H adsorption reaction, respectively. Herein, a solvation correction with energy equals to -0.22 eV is applied to only Δ

E_{*OH} and ΔE_{*OOH} since water molecule could solvate *OH and *OOH moieties with hydrogen bond, whereas the hydrogen bond is absent for *O. For OER intermediates, the adsorption Gibbs free energies can be expressed by Ref [5].

It is widely known that the OER is typical reversible reaction. It involves the four-electron transfer processes and elementary reactions pathways are displayed as following equations:

$$OH^- \xrightarrow{\Delta G1} * OH + e^- \quad (2)$$

$$* OH + OH^- \xrightarrow{\Delta G2} * O + H_2O + e^- \quad (3)$$

$$* O + OH^- \xrightarrow{\Delta G3} * OOH + e^- \quad (4)$$

$$* OOH + OH^- \xrightarrow{\Delta G4} O_2 + H_2O + e^- \quad (5)$$

where the "*" stand for the active adsorption site on catalysts.

According to the thermodynamics of OER, all the reaction steps are endothermic. The process with the largest endothermic process is the rate-determining step (RDS). The sample with the smallest U_L(OER) value has the highest OER catalytic activity, as described in the following equation:

$$U_L(\mathrm{OER}) = Max_i[\Delta G_i]/\mathrm{ne} - 1.23\ \mathrm{V} \quad (6)$$

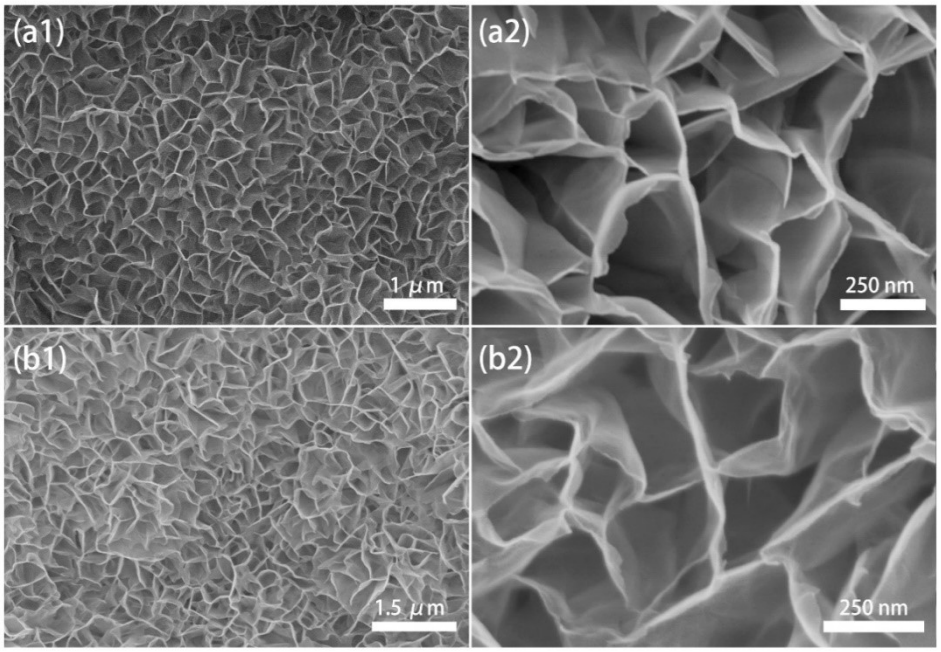

Fig. S1. SEM images of FeNi LDH (a1, 2) and (b1, 2) CM7-FeNi LDH.

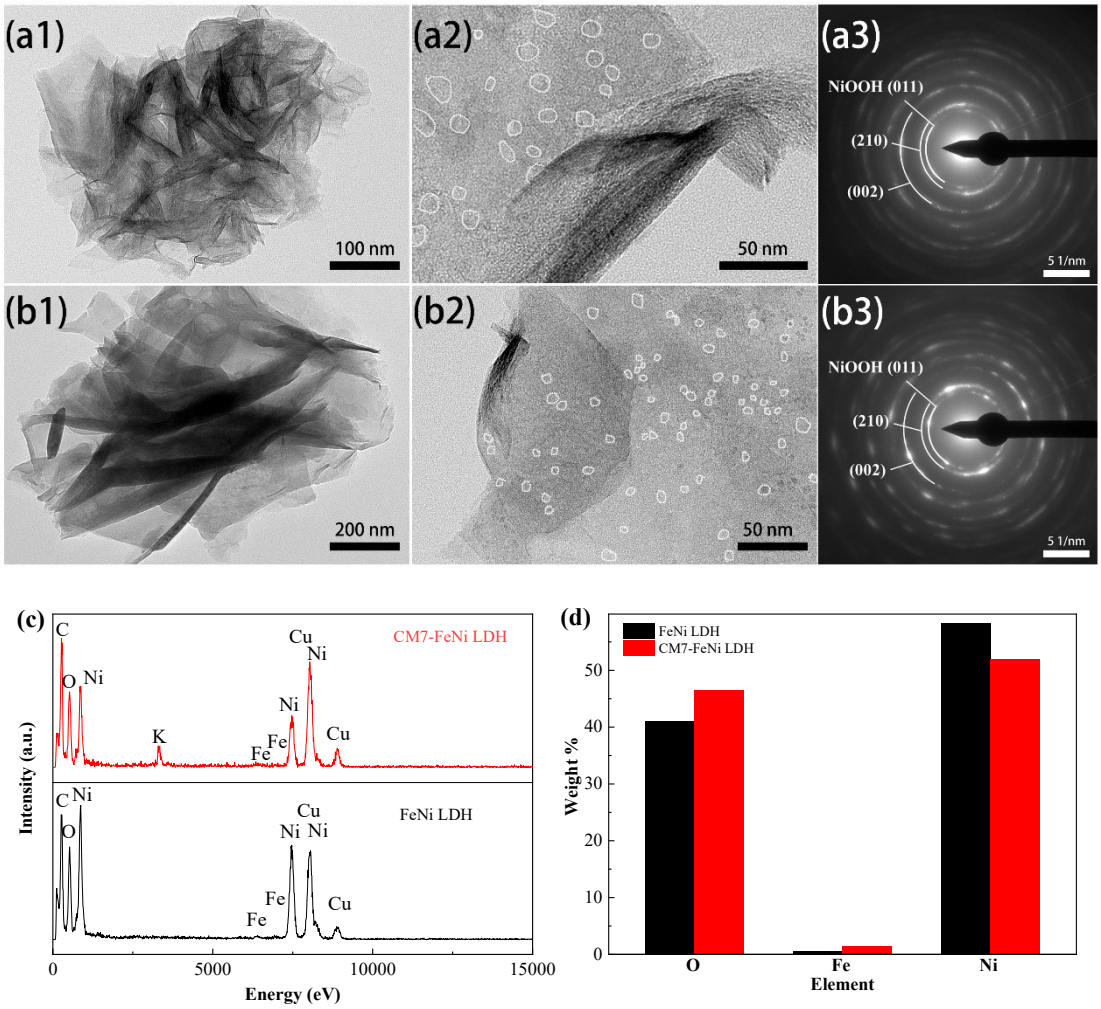

Fig. S2. TEM images and SAED patterns of (a) FeNi LDH and (b) CM7-FeNi LDH, (c) EDX and (d) element weight percentage of FeNi LDH and CM7-FeNi LDH.

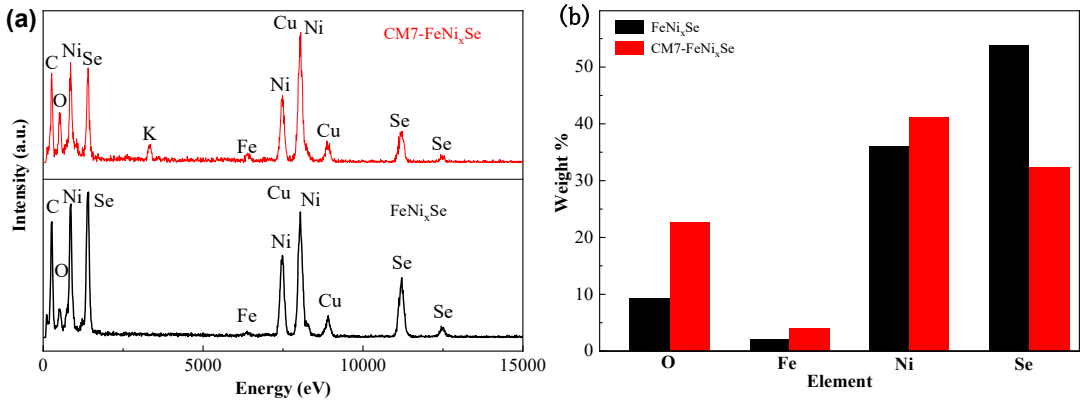

Fig. S3. (a) EDX and (b) percentage of element weight of CM7-FeNi$_x$Se and FeNi$_x$Se.

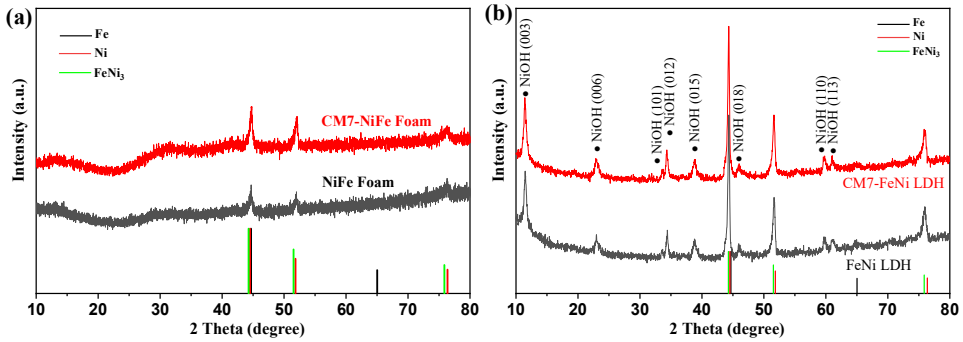

Fig. S4. (a) XRD patterns of NiFe Foam and CM7-NiFe Foam. (b) XRD patterns of FeNi LDH and CM7-FeNi LDH.

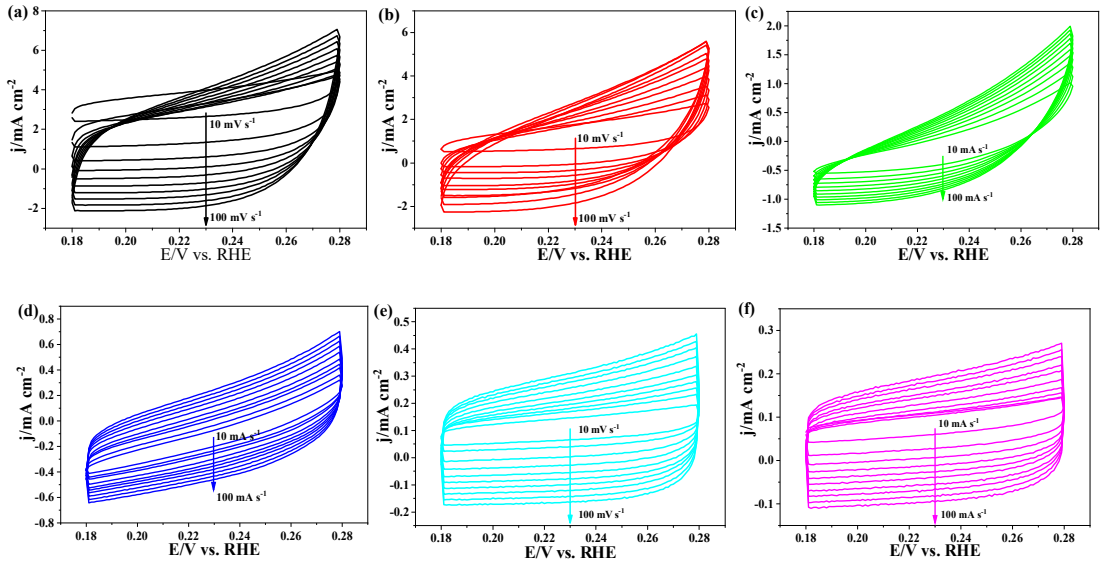

Fig. S5. CVs of (a) CM7-FeNi$_x$Se, (b) FeNi$_x$Se, (c) CM7-FeNi LDH, (d) FeNi LDH, (e) CM7-NiFe foam and (f) pure NiFe foam composite electrodes between the potential regions of 0.18 and 0.28 V (vs. RHE) with scan rates of 10, 20, 30, 40, 50, 60, 70 and 80 mV s^{-1} in 1.0 M KOH solution.

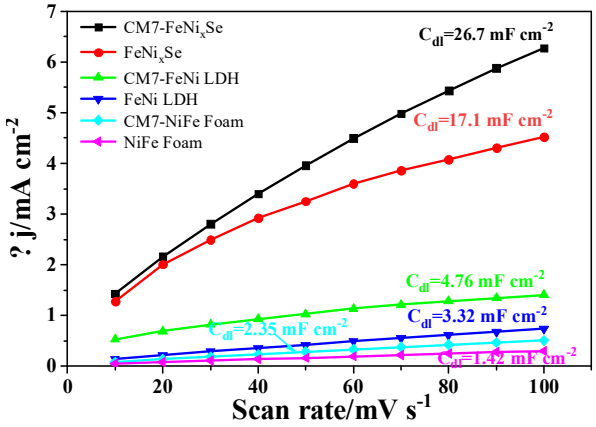

Fig. S6. Dependence of Δj on the scan rate at different double layer capacitances.

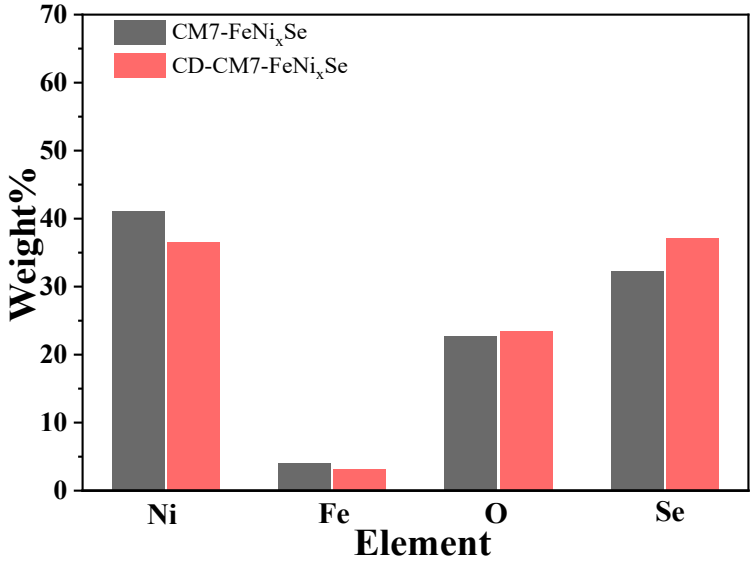

Fig. S7. Percentage of element weight of CD-CM7-FeNi$_x$Se and CM7-FeNi$_x$Se.

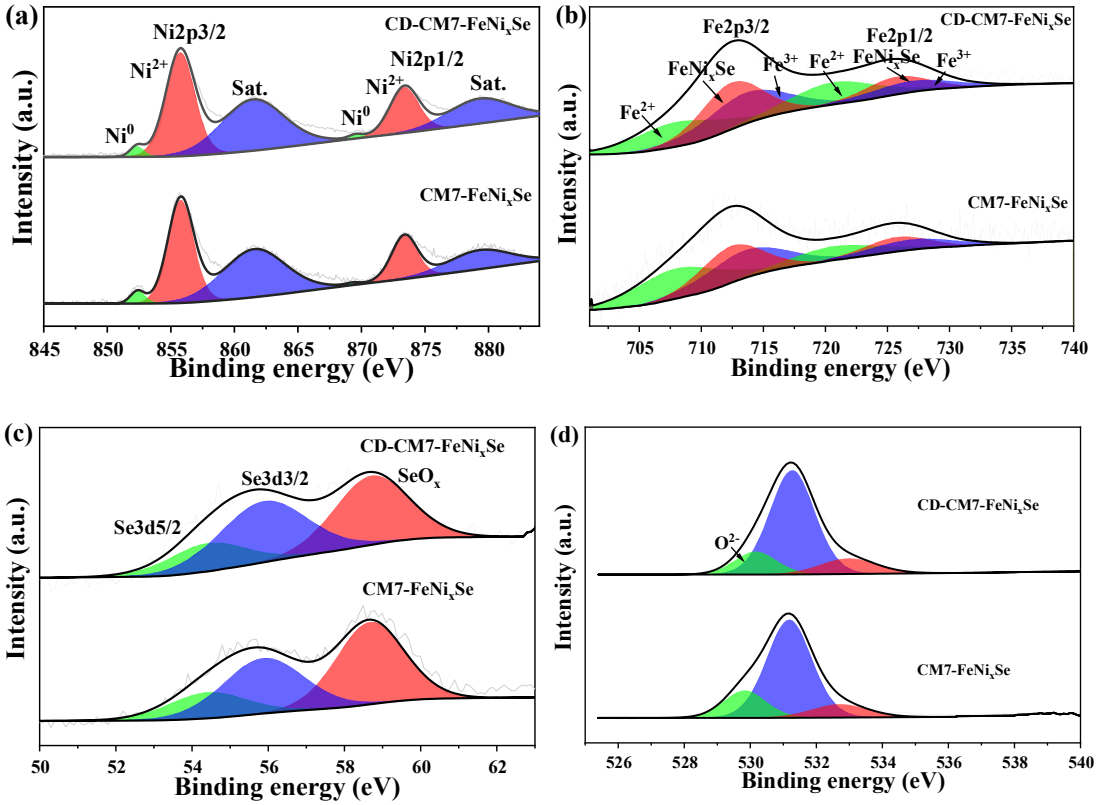

Fig. S8. High-resolution XPS spectra of (a) Ni 2p, (b) Fe2p, (c) Se3d and (d) O1s of the CM7-$FeNi_xSe$ and CM7-$FeNi_xSe$ after chronopotentiometry test (CD-CM7-$FeNi_xSe$) at constant current densities of 20 mA cm^{-2} by 10 h.

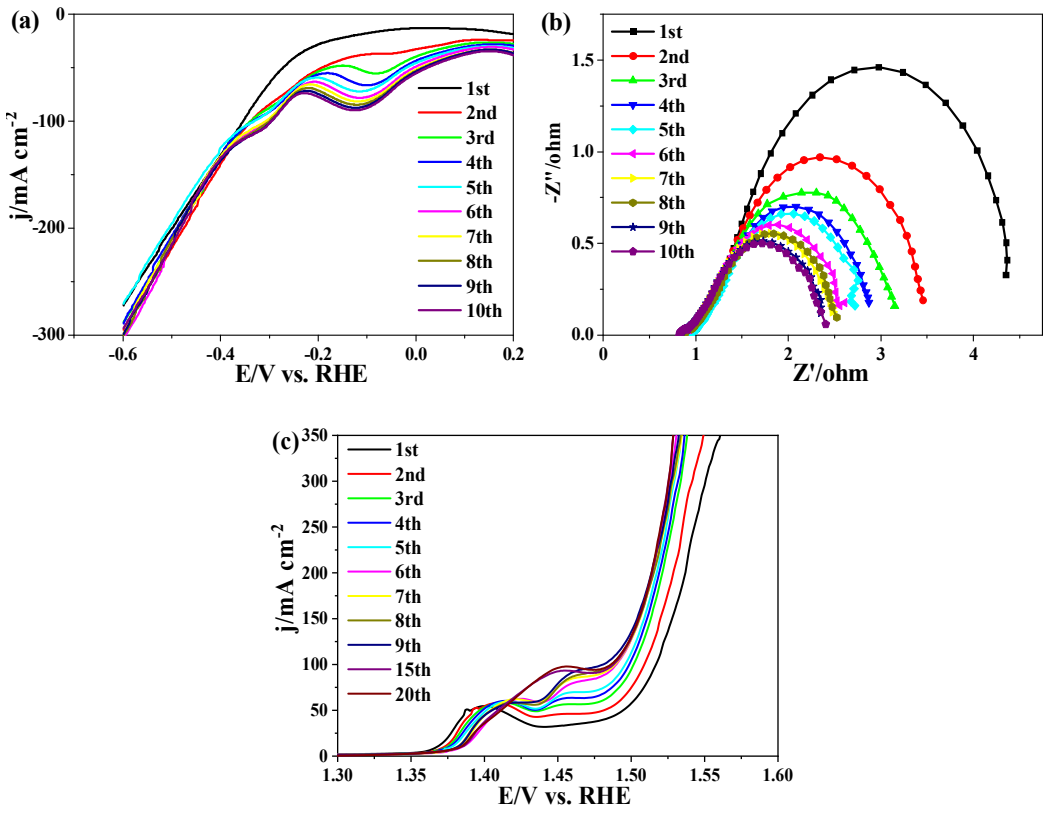

Fig. S9. (a) HER polarization curves, (b) Nyquist plots (overpotential=250 mV), and (c) OER polarization curves of CMy-FeNi$_x$Se (y represents HER cycle times), conducted in 1.0 M KOH.

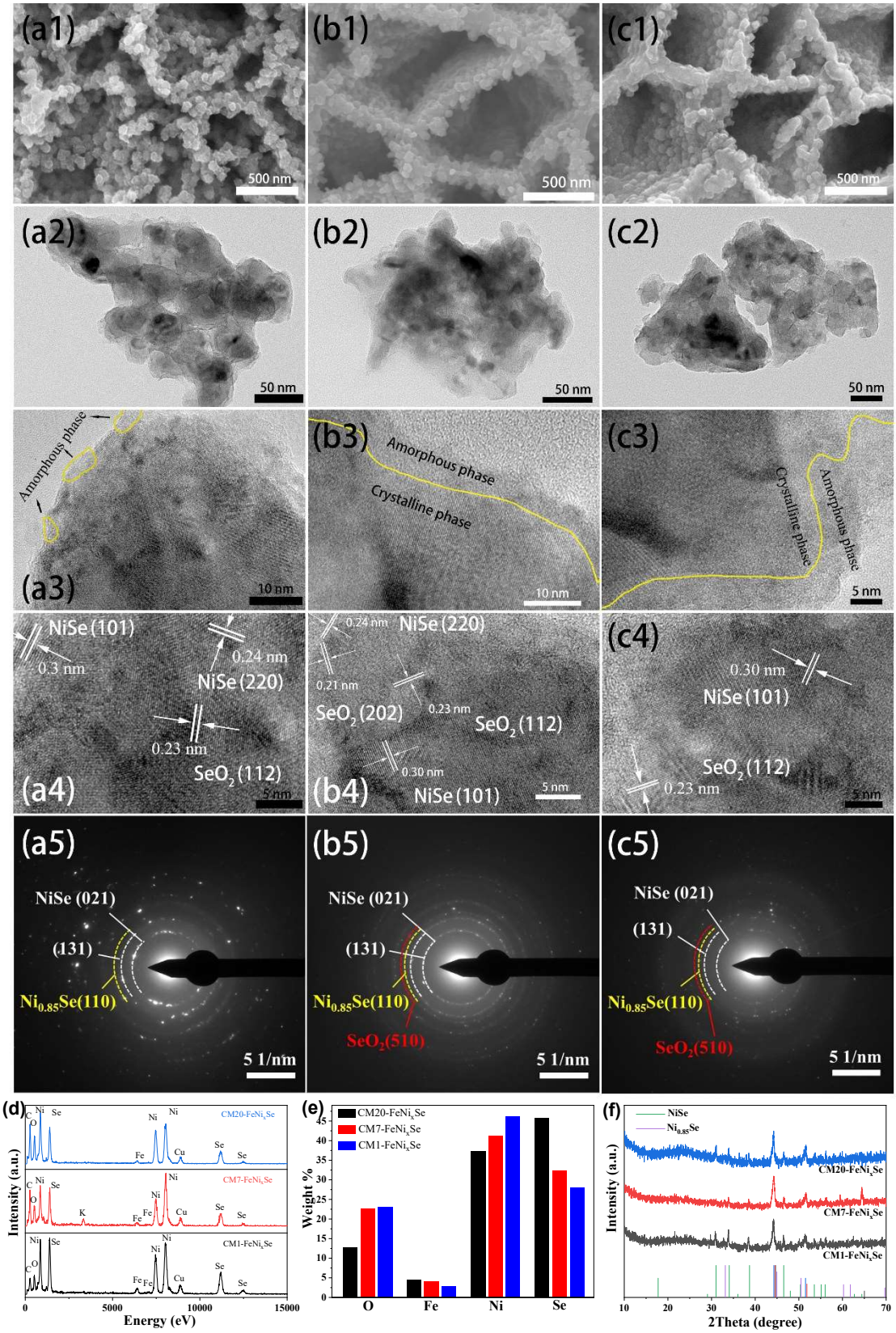

Fig. S10. SEM, TEM, HRTEM, SAED patterns of elements of (a1-5) CM1-FeNi$_x$Se, (b1-5) CM7-FeNi$_x$Se, (c1-5) CM20-FeNi$_x$Se; (d) EDX, (e) element weight percentage, and (f) XRD patterns of CM1-FeNi$_x$Se, CM7-FeNi$_x$Se, CM20-FeNi$_x$Se.

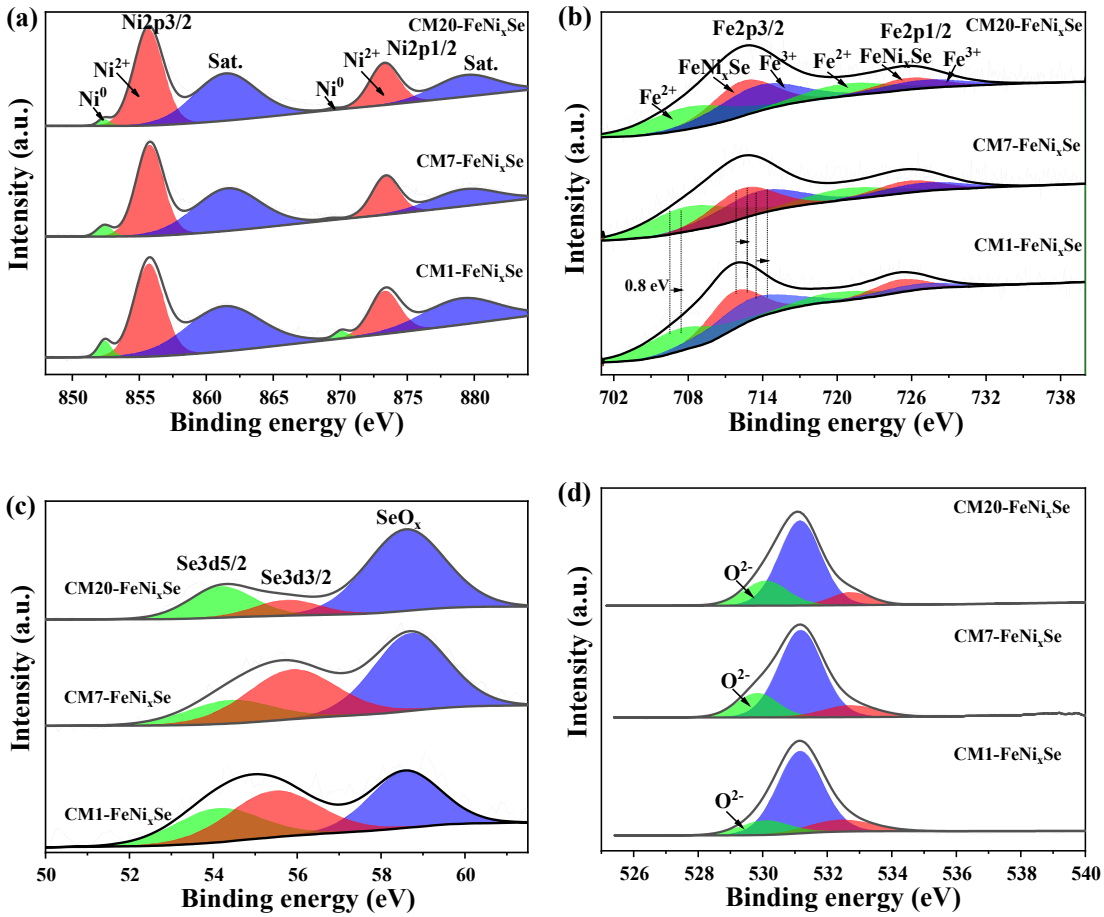

Fig. S11. High-resolution XPS spectra of (a) Ni 2p, (b) Fe2p, (c) Se3d and (d) O1s of the CM1-$FeNi_xSe$, CM7-$FeNi_xSe$ and CM20-$FeNi_xSe$.

Table S1. OER catalytic activity comparison of the CM7-FeNi$_x$Se with catalysts reported previously in the 1.0 M KOH.

Materials	Tafel Slope / mV dec^{-1}	η_{OER} / mV	References
SeO$_x$/FeNi$_x$Se	31	150 (10 mA cm^{-2}) 257 (100 mA cm^{-2}) 285 (200 mA cm^{-2})	This work
NiSe/Ni$_3$S$_2$	89	340 (100 mA cm^{-2})	6
Ni$_x$Fe$_{1-x}$Se$_2$	90	285 (10 mA cm^{-2})	7
NiSe$_2$/RGO	34	241 (10 mA cm^{-2})	8
O-NiSe@Ni/SS	48	290 (10 mA cm^{-2})	9
NiSe$_2$–CoSe$_2$/NCF	48	250 (10 mA cm^{-2})	10
Fe, Al-NiSe$_2$/rGO	48	272 (10 mA cm^{-2})	11
Mo–Ni–Se@NF	44	397 (100 mA cm^{-2})	12
MnSe@MOF-5/NF	61	170 (10 mA cm^{-2})	13
Se-MnS/NiS	50	317 (100 mA cm^{-2})	14
CoSe-0.2/NiSe-nrs/NF	58	310 (100 mA cm^{-2})	15
NiSe/NF	61	306 (100 mA cm^{-2})	16
NiSe$_2$	63	299 (10 mA cm^{-2})	17
NiSe-Ni$_{0.85}$Se/CP	98	300 (10 mA cm^{-2})	18
Fe–NiSe	43	220 (10 mA cm^{-2})	19

Table S2. Overall water splitting catalytic activity comparison of the Pt/C||CM7-FeNi$_x$Se with catalysts reported previously in 1.0 M KOH.

Materials	Overall water splitting η_{50}/ V	References
SeO$_x$/FeNi$_x$Se	1.64	This work
NiS$_{0.5}$Se$_{0.5}$	1.67	20
FeSe–NF	1.85	21
(Ni,Co)$_{0.85}$Se	1.87	22
Se-(NiCo)S/OH	1.86	23
A-NiSe$_2$|P	1.73	24
Se-MnS/NiS	1.66	14
Co(S$_{0.71}$Se$_{0.29}$)$_2$	1.82	25
hetero-Ni$_3$Se$_4$@NiFe LDH/CFC	1.71	26
Co-O@Co-Se	1.73	27
Ni$_{0.75}$Fe$_{0.25}$Se$_2$	1.69	28
Co$_{0.75}$Ni$_{0.25}$Se/NF	1.73	29
Fe$_{0.09}$Co$_{0.13}$-NiSe$_2$	1.63	30

References

1. J. Du, Z. Zou, C. Liu and C. Xu, *Nanoscale*, 2018, 10, 5163-5170.

2. G. Kresse and J. Furthmüller, *Phys. Rev. B*, 1996, 54, 11169-11186.

3. P. E. Blöchl, *Phys. Rev. B*, 1994, 50, 17953-17979.

4. M. C. Payne, M. P. Teter, D. C. Allan, T. A. Arias and J. D. Joannopoulos, *Rev. Mod. Phys.*, 1992, 64, 1045-1097.

5. C.-Y. Su, H. Cheng, W. Li, Z.-Q. Liu, N. Li, Z. Hou, F.-Q. Bai, H.-X. Zhang and T.-Y. Ma, *Adv. Energy Mater*, 2017, 7, 1602420.

6. L. Tie, Y. Liu, S. Shen, C. Yu, J. Sun and J. Sun, *Appl. Surf. Sci.*, 2020, 526, 146745.

7. Y. Li, R. Chen, D. Yan and S. Wang, *Chem.-Asian J.*, 2020, 15, 3845-3852.

8. P. Wei, Z. Hao, Y. Yang, M. Liu, H. Zhang, M.-R. Gao and S.-H. Yu, *Nano Res.*, 2020, 13, 3292-3298.

9. Y.-Y. Sun, Y.-X. Zhu, L.-K. Wu, G.-Y. Hou, Y.-P. Tang, H.-Z. Cao and G.-Q. Zheng, *Electrochim. Acta*, 2020, 353, 136519.

10. D. Chen, Z. Xu, W. Chen, G. Chen, J. Huang, C. Song, C. Li and K. Ostrikov, *J. Mater. Chem. A*, 2020, 8, 12035-12044.

11. L. Chen, H. Jang, M. G. Kim, Q. Qin, X. Liu and J. Cho, *Nanoscale*, 2020, 12, 13680-13687.

12. H. Yang, Y. Huang, W. Y. Teoh, L. Jiang, W. Chen, L. Zhang and J. Yan, *Electrochim. Acta*, 2020, 349, 136336.

13. M. Fiaz and M. Athar, *JOM*, 2020, 72, 2219-2225.

14. J. Zhu, M. Sun, S. Liu, X. Liu, K. Hu and L. Wang, *J. Mater. Chem. A*, 2019, 7, 26975-26983.

15. J. Du, S. You, X. Li, B. Tang, B. Jiang, Y. Yu, Z. Cai, N. Ren and J. Zou, *ACS Appl. Mater. Interfaces*, 2020, 12, 686-697.

16. S. Esmailzadeh, T. Shahrabi, G. Barati Darband and Y. Yaghoubinezhad, *Electrochim. Acta*, 2020, 334, 135549.

17. C. Cai, Y. Mi, S. Han, Q. Wang, W. Liu, X. Wu, Z. Zheng, X. Xia, L. Qiao, W. Zhou and

X. Zu, *Electrochim. Acta*, 2019, 295, 92-98.

18. Y. Chen, Z. Ren, H. Fu, X. Zhang, G. Tian and H. Fu, *Small*, 2018, 14, 1800763.
19. B. Xu, Z. Chen, X. Yang, X. Wang, Y. Huang and C. Li, *Chem. Commun.*, 2018, 54, 9075-9078.
20. Y. Wang, X. Li, M. Zhang, Y. Zhou, D. Rao, C. Zhong, J. Zhang, X. Han, W. Hu, Y. Zhang, K. Zaghib, Y. Wang and Y. Deng, *Adv. Mater.*, 2020, 32, 2000231.
21. D. Chanda, R. A. Tufa, Y. Y. Birdja, S. Basu and S. Liu, *Int. J. Hydrogen Energy*, 2020, 45, 27182-27192.
22. K. Xiao, L. Zhou, M. Shao and M. Wei, *J. Mater. Chem. A*, 2018, 6, 7585-7591.
23. C. Hu, L. Zhang, Z.-J. Zhao, A. Li, X. Chang and J. Gong, *Adv. Mater.*, 2018, 30, 1705538.
24. J. Lin, H. Wang, J. Cao, F. He, J. Feng and J. Qi, *J. Colloid Interf. Sci.*, 2020, 571, 260-266.
25. L. Fang, W. Li, Y. Guan, Y. Feng, H. Zhang, S. Wang and Y. Wang, *Adv. Funct. Mater.*, 2017, 27, 1701008.
26. T. Zhang, L. Hang, Y. Sun, D. Men, X. Li, L. Wen, X. Lyu and Y. Li, *Nanoscale Horiz.*, 2019, 4, 1132-1138.
27. W. Q. Yang, Y. X. Hua, Q. B. Zhang, H. Lei and C. Y. Xu, *Electrochim. Acta*, 2018, 273, 71-79.
28. X. Hu, Q. Zhou, P. Cheng, S. Su, X. Wang, X. Gao, G. Zhou, Z. Zhang and J. Liu, *Appl. Surf. Sci.*, 2019, 488, 326-334.
29. S. Liu, Y. Jiang, M. Yang, M. Zhang, Q. Guo, W. Shen, R. He and M. Li, *Nanoscale*, 2019, 11, 7959-7966.
30. Y. Sun, K. Xu, Z. Wei, H. Li, T. Zhang, X. Li, W. Cai, J. Ma, H. J. Fan and Y. Li, *Adv. Mater.*, 2018, 30, 1802121.